Article

Neuron

A Fully Automated Approach to Spike Sorting

Highlights

- MountainSort is a new fully automated spike sorting algorithm and software package
- Accuracy is comparable to or greater than that of existing methods
- Desktop computation speeds are ~70/30/2.5× real time for 4/16/128 electrodes
- The software enables reproducible spike sorting for large datasets

Authors

Jason E. Chung, Jeremy F. Magland, Alex H. Barnett, ..., Sarah H. Felix, Loren M. Frank, Leslie F. Greengard

Correspondence

loren@phy.ucsf.edu

In Brief

Chung, Magland, et al. present MountainSort, a new fully automatic spike sorting package with a powerful GUI. MountainSort has accuracy comparable to current methods and runtimes faster than real time, enabling automatic and reproducible spike sorting for high-density extracellular recordings.

Chung et al., 2017, Neuron *95*, 1381–1394
September 13, 2017
http://dx.doi.org/10.1016/j.neuron.2017.08.030

CellPress

Neuron
Article

A Fully Automated Approach to Spike Sorting

Jason E. Chung,[1,9] Jeremy F. Magland,[2,9] Alex H. Barnett,[2,4] Vanessa M. Tolosa,[5,7] Angela C. Tooker,[5] Kye Y. Lee,[5] Kedar G. Shah,[5,8] Sarah H. Felix,[5] Loren M. Frank,[1,6,10,*] and Leslie F. Greengard[2,3]
[1]Neuroscience Graduate Program, Kavli Institute for Fundamental Neuroscience and Department of Physiology, University of California San Francisco, CA 94158, USA
[2]Center for Computational Biology, Flatiron Institute, 162 Fifth Avenue, New York, NY 10010, USA
[3]Courant Institute, NYU, New York, NY 10012, USA
[4]Department of Mathematics, Dartmouth College, Hanover, NH 03755, USA
[5]Center for Micro- and Nano-Technology, Lawrence Livermore National Laboratory, Livermore, CA 94550, USA
[6]Howard Hughes Medical Institute
[7]Present address: Neuralink Corp., San Francisco, CA 94107, USA
[8]Present address: Verily Life Sciences, 269 E. Grand Avenue, South San Francisco, CA 94080, USA
[9]These authors contributed equally
[10]Lead Contact
*Correspondence: loren@phy.ucsf.edu
http://dx.doi.org/10.1016/j.neuron.2017.08.030

SUMMARY

Understanding the detailed dynamics of neuronal networks will require the simultaneous measurement of spike trains from hundreds of neurons (or more). Currently, approaches to extracting spike times and labels from raw data are time consuming, lack standardization, and involve manual intervention, making it difficult to maintain data provenance and assess the quality of scientific results. Here, we describe an automated clustering approach and associated software package that addresses these problems and provides novel cluster quality metrics. We show that our approach has accuracy comparable to or exceeding that achieved using manual or semi-manual techniques with desktop central processing unit (CPU) runtimes faster than acquisition time for up to hundreds of electrodes. Moreover, a single choice of parameters in the algorithm is effective for a variety of electrode geometries and across multiple brain regions. This algorithm has the potential to enable reproducible and automated spike sorting of larger scale recordings than is currently possible.

INTRODUCTION

Advances in our understanding of how populations of neurons represent and process information has been enabled by tightly packed multi-electrode arrays that allow for isolation of large numbers of simultaneously recorded neurons (Csicsvari et al., 2003; Gray et al., 1995; Lopez et al., 2016; McNaughton et al., 1983). Data collected from these devices comprise multiple channels of continuously sampled extracellular voltages. A key step in making these data interpretable is spike sorting, the process of detecting spiking events and assigning those events to single units corresponding to putative individual neurons (Einevoll et al., 2012; Harris et al., 2016; Lewicki, 1998; Muller, 1996; Quiroga, 2012).

A number of challenges make spike sorting more complex than clustering in many other disciplines. First, there is no simple noise model. The background signal arises from the combinations of multiple complex signals, including small spikes from hundreds of distant neurons, and can contain electrical noise mixed with true neural signals (Einevoll et al., 2012). Second, variation in waveform shapes for a given cell can be highly non-Gaussian and skewed, particularly when bursting occurs (Harris et al., 2001; Quirk et al., 2001; Quirk and Wilson, 1999) or when the cell positions drift over time relative to the physical electrode (Bar-Hillel et al., 2006; Calabrese and Paninski, 2011; Chestek et al., 2007; Emondi et al., 2004). Multiple neurons may fire simultaneously, leading to time-overlapping spike signals, and, while this may not occur frequently in some brain areas or with small electrode arrays, for large arrays sampling tens to hundreds of neurons, individual spikes will often time-overlap with other events (Ekanadham et al., 2014; Franke et al., 2010).

The majority of spike sorting algorithms comprise a sequence of steps such as band-pass filtering, spatial whitening, detection of threshold-crossing events, and clustering based on voltage waveform shape in a suitable feature space; this generally involves one or more manual processing steps (Einevoll et al., 2012; Lewicki, 1998; Marre et al., 2012; Quiroga, 2012). At one extreme, the clustering itself is performed by a human operator, viewing the event features in two-dimensional projections, and drawing cluster boundaries with the assistance of specialized user interfaces (Xclust, M.A. Wilson; MClust, A.D. Redish; Offline Sorter, Plexon). In other situations, clustering is automated, but the user must curate the results by selecting which clusters to reject, merge, or even split (Hill et al., 2011; Kadir et al., 2014; Rossant et al., 2016). There also exist post-processing steps that resolve overlapping spikes (Ekanadham et al., 2014; Franke et al., 2015; Pachitariu et al., 2016; Pillow et al., 2013) and algorithms based on independent component analysis (ICA) that do

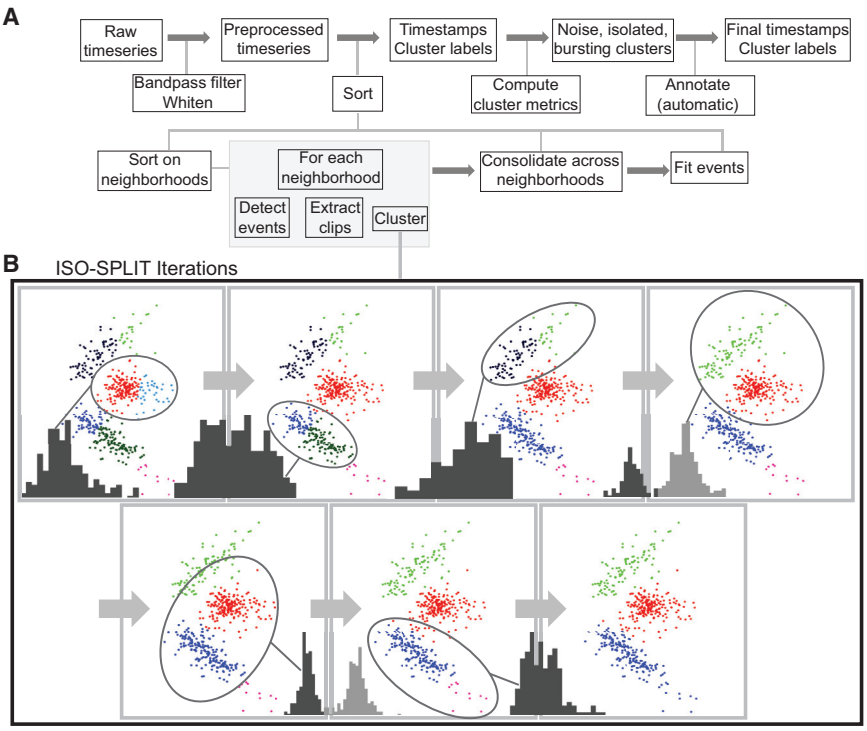

Figure 1. Overview of the Fully Automated MountainSort Processing Pipeline

(A) Flow diagram. After preprocessing, sorting is performed on individual electrode neighborhoods. Clusters are then consolidated across neighborhoods (see also Figure S1). Clusters are either accepted or rejected in the automatic annotation phase based on the computed cluster metrics.

(B) Illustration of the final six iterations of the ISO-SPLIT clustering algorithm for a synthetically generated set of points. At each iteration, two clusters are compared using a one-dimensional projection of the union of the two clusters (shown in the histograms at each iteration). The ISO-CUT procedure is applied to the projected data to determine whether the two clusters should be merged (single color in the histogram) or whether the points should be redistributed according to an optimal cut point (two colors in the histogram).

not explicitly involve clustering (Takahahi et al., 2002). Presently, despite many available packages and proposed algorithms, no generally adopted software packages offer fully automated sorting that can take in the raw time series data and output spike times and identities without the expectation of further curation.

From the standpoint of efficient and reproducible science, any human intervention has disadvantages. Manual sorting can have error rates in excess of 20% (Wood et al., 2004), and there is substantial variability in labeling across different sorting sessions (Harris et al., 2000; Pedreira et al., 2012; Rossant et al., 2016). Furthermore, the human spike sorter could never keep up with the increasing volume of data arising from increasingly large electrode arrays applied over increasingly long durations (Berényi et al., 2014; Dhawale et al., 2015; Du et al., 2011; Lopez et al., 2016; Santhanam et al., 2007; Shobe et al., 2015).

Although fully automated spike sorting has been of interest for many years (Abeles and Goldstein, 1977), and despite prior efforts to automate sorting algorithms (Calabrese and Paninski, 2011; Carlson et al., 2014; Einevoll et al., 2012; Ekanadham et al., 2014; Franke et al., 2010, 2015; Kadir et al., 2014; Lewicki, 1998; Marre et al., 2012; Pillow et al., 2013; Quiroga et al., 2004; Rodriguez and Laio, 2014; Swindale and Spacek, 2014; Takekawa et al., 2012), the majority of laboratories still rely heavily on manual intervention. In this work, we set out to develop a fully automated spike sorting algorithm having error rates that are comparable to or lower than those of existing manual and semi-manual approaches, and with runtimes faster than acquisition times. We introduce MountainSort, a novel spike sorting algorithm and open-source software suite of processing, visualization, and curation tools.

RESULTS

A central goal of our overall spike sorting strategy has been to develop a single algorithm that can be applied to data from different brain regions without the need for brain-region specific models or parameters. This requires that the procedure be insensitive to differences in dataset properties such as non-Gaussian cluster distributions, electrode densities, and firing rates. Further, selecting parameters such as thresholds and regularization constants is time consuming and can call into question the objectivity of results. Therefore, our guiding philosophy is to minimize both the number of user-defined parameters and the number of modeling assumptions, while maintaining high spike sorting accuracy and efficiency.

To satisfy these requirements, we developed the spike sorting pipeline shown in Figure 1A. This involves preprocessing, sorting on electrode neighborhoods, consolidation across those neighborhoods, fitting, derivation of cluster metrics, and automated annotation based on those metrics. The last step replaces manual curation (deciding on which clusters to accept) but importantly does not involve corrections to clustering as with other approaches. Details of all processing steps are provided in STAR Methods. Here, we give an overview of the most critical steps.

Clustering of Neural Events

At the heart of our sorting pipeline is a new, efficient, nonparametric, density-based clustering algorithm termed ISO-SPLIT (Figure 1B), used to sort spike events based on their representations in a low-dimensional feature space. The algorithm makes only two general assumptions about cluster distributions in this space. First, we assume that each cluster arises from a density function that, when projected onto any line, is unimodal, having a single region of highest density. Second, we assume that any two distinct clusters may be separated by a hyperplane, in the neighborhood of which there is a relatively lower density. In our

experience, the unimodality hypothesis appears to hold for the large majority of neurons taken from a variety of brain areas—this assumption is also implicit in most neural clustering methods, even those that do not assume a Gaussian shape (Fee et al., 1996; Quiroga et al., 2004; Vargas-Irwin and Donoghue, 2007). In a minority of cases, we have observed a multimodal cluster distribution, reflecting more complex firing properties of a single neuron. Our strategy for handling this challenging scenario is discussed below.

Technical details for ISO-SPLIT are provided in STAR Methods. The algorithm comprises a series of nonparametric statistical tests for unimodality and makes no assumptions about the shapes of clusters aside from having unimodal one-dimensional projections. It therefore involves few adjustable parameters. Essentially one needs only to specify a statistical threshold for rejecting the null hypothesis of unimodality; the clustering output is largely insensitive to this threshold due to the test being repeated at every iteration. The method is also insensitive to the initialization (see STAR Methods). We use the same set of parameters for all examples in this study. Moreover, the algorithm needs no a priori information about the expected number of clusters nor the expected cluster densities.

Sorting Large Electrode Arrays

As indicated in Figure 1, sorting is first performed independently on electrode neighborhoods (one neighborhood per electrode) based on the geometric layout of the array. Redundant clusters are then removed during the next phase entitled "consolidation across neighborhoods" (Figure S1). There are a number of advantages of using such a consolidation approach rather than a more error-prone merging procedure (see STAR Methods). Importantly, this approach allows scaling to very large electrode arrays as the neighborhood sizes will remain roughly constant.

Identification of Putative "Single-Unit," "Noise," "Non-isolated," and "Bursting" Clusters

As part of the overall automation, we developed metrics for determining which clusters are sufficiently isolated from noise and other clusters to be included in the final output. In this way only sufficiently isolated clusters are selected for downstream analysis. Our quality assessment categorizes the clusters into three groups: "single unit," "noise," and "non-isolated." In addition, we automatically identify (based on timing information) clear cases where the events of a bursting unit are split into multiple unimodal clusters (see STAR Methods). Such decisions have traditionally been handled via case-by-case curation by manual operators. In contrast, our strategy only requires the operator to set thresholds on cluster quality metrics, as defined below. These metrics can be adjusted based on the type of analysis that will be done. Furthermore, the metrics can also be exported alongside the event times and labels, allowing analyses sensitive to unit isolation and noise contamination to be repeated with different thresholds or weighting criteria.

As stated, a central goal of our approach is to minimize the number of modeling assumptions. Currently available metrics (Harris et al., 2001; Schmitzer-Torbert et al., 2005; Schmitzer-Torbert and Redish, 2004), while useful, make assumptions about an underlying noise model. Here, we introduce two new metrics that make no such assumptions and are specifically suited to spike sorting: isolation and noise overlap. We also use a measure of cluster signal-to-noise (SNR) to exclude clusters contaminated by artifacts and employ a timing criterion to flag bursting situations.

Isolation

The isolation metric quantifies how well separated (in feature space) the cluster is from other nearby clusters. Clusters that are not well separated from others would be expected to have high false-positive and false-negative rates due to mixing with overlapping clusters. This quantity is calculated in a nonparametric way based on nearest-neighbor classification.

Noise Overlap

Noise overlap estimates the fraction of "noise events" in a cluster, i.e., above-threshold events not associated with true firings of this or any of the other clustered units. A large noise overlap implies a high false-positive rate. The procedure first empirically computes the expected waveform shape for noise events that have by chance crossed the detection threshold. It assesses the extent of feature space overlap between the cluster and a set of randomly selected noise clips after correcting for this expected noise waveform shape.

The noise overlap and isolation metrics vary between 0 and 1, and in a sense, represent the fraction of points that overlap either with another cluster (isolation metric) or with the noise cluster (noise overlap metric). However, they should *not* be interpreted as a direct estimate of the misclassification rate but should rather be considered to be predictive of this quantity. Indeed, due to the way they are computed, these values will depend on factors such as the dimensionality of the feature space and the noise properties of the underlying data. Therefore, the annotation thresholds should be chosen to suit the application. With that said, in this study we used the same sorting parameters and annotation thresholds for all analyses.

Cluster SNR

Depending on the nature of signal contamination in the dataset, some clusters may consist primarily of high-amplitude artifactual signals such as those that arise from movement, muscle, or other non-neural sources. In this case, the variation among event voltage clips will be large compared with clusters that correspond to neural units. To automatically exclude such clusters we compute cluster SNR, defined as the peak absolute amplitude of the average waveform divided by the peak SD. The latter is defined as the SD of the aligned clips in the cluster, taken at the channel and time sample where this quantity is largest.

Bursting Units

While events corresponding to a single unit almost always form a cluster that is well approximated by a unimodal distribution, there are instances where the underlying distribution is multimodal. From our data we see that this most often occurs when the first spike in a burst has a different shape and higher amplitude than subsequent spikes in the burst. Our sorting algorithm by design will separate these events into two or more clusters. Fortunately, such clusters can be readily identified using event timing information, as the smaller spikes will always occur within a short time after the first spike in the burst. In the case of our hippocampal data, this time window is on the order

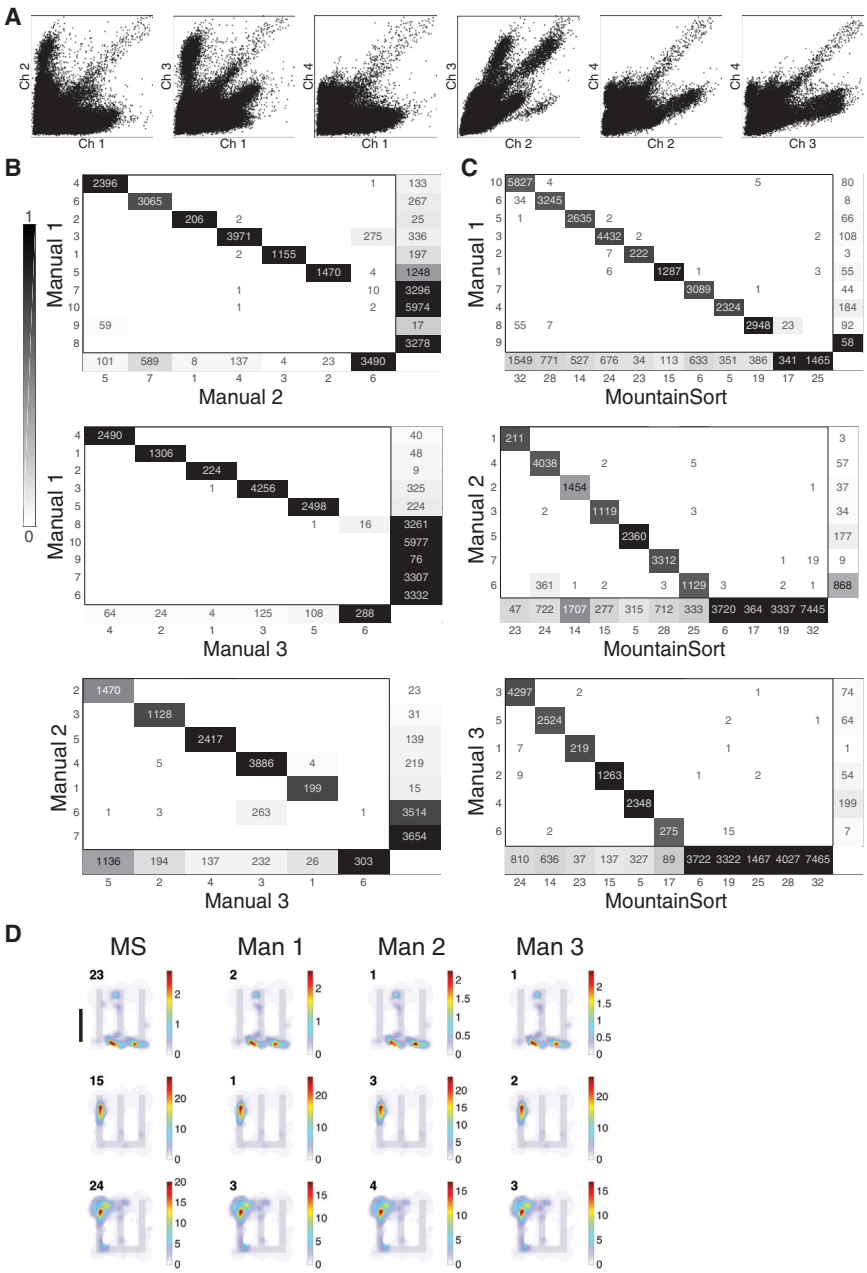

Figure 2. Fully Automated MountainSort Produces Clusters Comparable to Manual Operators

(A) Two-dimensional peak amplitude projections of the data used for manual sorting. Axes show values between 0 and 500 μv.

(B) Pairwise confusion matrices (Figure S2A) for the three manual sortings. For each matrix, the numbers in the leftmost column and bottommost row correspond to cluster ID number for the respective manual sorter. Shading corresponds to the proportion of each column-labeled cluster that is classified into each row-labeled cluster. For the top matrix, this is the proportion of events in each manual 2 cluster that match the corresponding manual 1 cluster. Each number within the matrix corresponds to the absolute number of matching events. The final column corresponds to the number of events found in the row-labeled clustering not found in the column-labeled clustering. For the top matrix, this corresponds to the events in manual 1 clusters that are not found in any manual 2 clusters. Similarly, the second row from the bottom corresponds to the number of events found in the manual 2 clusters not found in any manual 1 clusters.

(C) As in (B), except for purpose of compact visualization, only the MountainSort clusters that correspond to one or more manual clusters are shown.

(D) Occupancy-normalized spatial firing rate color maps for three clusters corresponding across MountainSort (MS) and manual operators. See also Figure S2. Track outline is shown in gray. Note that the track has no walls, and we used the animal's head for position tracking. As the animal often looked out over the edge of the track, many of the positions shown are outside the track outline. Scale bar, 50 cm. Note that color-bar scale varies across clusters.

of 15 ms (Harris et al., 2001). In the STAR Methods, we describe the criteria used to label a cluster as having a ''bursting parent'' cluster.

Comparison to Manual Clustering for a Tetrode Dataset

If automated spike sorting is to be useful, it should provide cluster labels with accuracy comparable to or exceeding existing standards. We therefore began with a comparison of our automated approach to manual sorting for a dataset that poses serious spike sorting challenges: tetrode recordings from the CA1 region of rat hippocampus (Figure 2A). The pyramidal cells in CA1 are densely packed, and thus large numbers of cells can be detected on the same electrode. Furthermore, extracellular recordings from single CA1 neurons show substantial waveform variability as a result of bursting and other history-dependent effects (Harris et al., 2001; Quirk et al., 2001). We chose a dataset with some electrode drift (45-min recording session) and some artifact contamination resulting from animal movement. The data were derived from a novel exposure to a spatial environment where we expected to see neurons changing their firing rates substantially over time (Frank et al., 2004; Wilson and McNaughton, 1993). The standard in the field for such datasets is either fully manual clustering, or semi-automatic clustering where the algorithm over-clusters the data leaving the user to manually merge clusters or redraw cluster boundaries (Rossant et al., 2016).

Three different manual operators clustered the dataset using drawn polygons across several different 2D projections (see STAR Methods). As expected (Harris et al., 2000), while there

were clusters that all three operators identified, there was variability across operators, both in which clusters were sufficiently isolated to merit inclusion, as well as in the placement of the boundaries separating clusters, resulting in a range of unmatched events in each cluster (Figure 2B). MountainSort was then run; results of the comparison are shown in the confusion matrices of Figure 2C. A confusion matrix (or contingency table; Zaki and Meira, 2014) summarizes the consistency between two sortings of the same data by showing the pairwise counts (Figure S2A). The entry a_{ij} represents the number of events that were classified as i in the first sorting and as j in the second. To handle the arbitrary ordering of labels, the rows and columns are permuted to maximize the sum of the diagonal entries (Kuhn, 1955). A purely diagonal matrix corresponds to perfect agreement. For compact visualization, 11 of the 24 automatically sorted MountainSort clusters with the best match to the manual sorting results are shown.

As shown in Figure 2C, all six clusters that are identified in two or more manual clusterings are also identified by MountainSort (MountainSort labels 23, 15, 24, 5, 14/16, 28). For example, MountainSort cluster 24 corresponds to clusters 3, 4, and 3 in the first, second, and third manual sortings, respectively, with more than 97% of the manual events also detected by MountainSort. At the same time, MountainSort identifies a large number of events as part of these clusters that are not included in the manual sortings (Figure 2C). That is not surprising given that our approach to manual clustering aims to minimize the mistaken inclusion of incorrect events at the expense of missing true events; this approach was chosen because false-positives can lead to incorrect inferences about correlated activity (Quirk and Wilson, 1999).

Are these additional events likely to be true spiking events associated with the cell? Ground truth is not available for this dataset, or for the vast majority of other datasets, but in this case we can take advantage of the well-known "place fields" of hippocampal neurons (O'Keefe and Dostrovsky, 1971) to infer the accuracy of the sorting. We therefore examined the animal's location at the times the spikes were detected. If the additional events are correctly classified, then they should congregate in the same location as the bulk of the events. This is indeed the case. As shown in Figures 2D and S2B, events detected by MountainSort but not by manual operators have spatial distributions very similar to those of the jointly detected or individually detected events, suggesting that these additional events are likely to be correctly assigned to this cluster.

MountainSort also identifies a large number of clusters that were not identified by the manual sorters. For the tetrode data featured in Figure 2, we used the following metric thresholds: noise overlap <0.03, isolation >0.95, firing rate >0.1 Hz, SNR >1.5, although identical classifications for this dataset would result from using only noise overlap and firing rate. After automated curation and one automated bursting-related cluster merge (below), this resulted in the identification of 24 putative single units (Figure 3A). Importantly, these isolated clusters have few, if any, refractory period violations even though MountainSort does not use time information for clustering decisions (Figure 3B). Furthermore, 22 of the 24 putative single units have spatially restricted firing properties, consistent with expected behavior from hippocampal CA1 principal cells (Figure 3C). MountainSort clusters 12 and 21 do not have spatially restricted firing properties and are relatively low amplitude; however, both have few refractory period violations and also have noise overlap scores that are below threshold (0.01 and 0.02, respectively; noise overlap threshold = 0.03). Further, the high firing rates of these units suggest that they are likely to correspond to one of the subtypes of inhibitory interneurons that can be found near the CA1 cell layer (Freund and Buzsáki, 1996).

We further evaluated the quality of the isolation of these additional units by identifying the cluster pairs that had the most similar waveforms, as quantified by isolation score, and asking whether there was evidence of contamination or low-quality clustering in those pairs. In this dataset, clusters 7 and 9 have the lowest isolation score of 0.96, and clusters 6 and 4 have the next lowest, an isolation score of 0.97. Despite these lower isolation scores, both pairs of clusters have noticeable waveform differences, clear separation in the principal component (PC) space, and a difference in spatial firing preferences (Figures S3A and S3B). This suggests that these clusters all represent well-isolated single units that likely correspond to single neurons.

Overall, we found that an isolation score <0.99 could reflect either activity originating from at least two different neurons (Figures S3A and S3B) or activity from a single, bursting neuron with substantial amplitude variation and a multimodal cluster distribution. One such bursting cluster pair was automatically identified in this dataset (Figures S3C and S3D cluster labels 14, 16; isolation = 0.97). Examination of their respective waveforms shapes, spatial firing properties (Figure S3C), and cross-correlation (Figure S3D), suggest that the two clusters come from a bursting neuron, with the higher amplitude cluster often spiking before the lower-amplitude cluster. Indeed, after an automatic merge of MountainSort clusters 14 and 16 based on an identification of burst pairs (see STAR Methods), we find strong similarity to manually identified clusters (manual 1 cluster 5, manual 2 cluster 2, manual 3 cluster 5, Figure S2B). Here, we note that automatically joining these two clusters required adding assumptions about relative spike timing and amplitudes into the post-clustering automated annotation stage. Nonetheless, while the merge is done in an automated fashion, the software maintains a record of that annotation alongside the original cluster assignments. This makes it straightforward for other scientists to assess all annotations made during sorting.

Five clusters were tagged as overlapping with noise (using noise overlap >0.03). Visual inspection of the events in these clusters revealed four of the five having of broad and symmetric waveforms (Figure S3E), characteristic of what one might expect from the summation of activity from many distant neurons crossing the event detection threshold. Furthermore, all five of these clusters have events falling in the refractory period, suggesting that the noise overlap measure effectively identifies clusters with events that should indeed be considered noise (Figure S3F). In summary, the findings above indicate that MountainSort can produce high-quality automatic sorting of tetrode datasets.

Finally, it is worth noting that only one of the isolated units was able to be identified on the basis of the individual channel sorting.

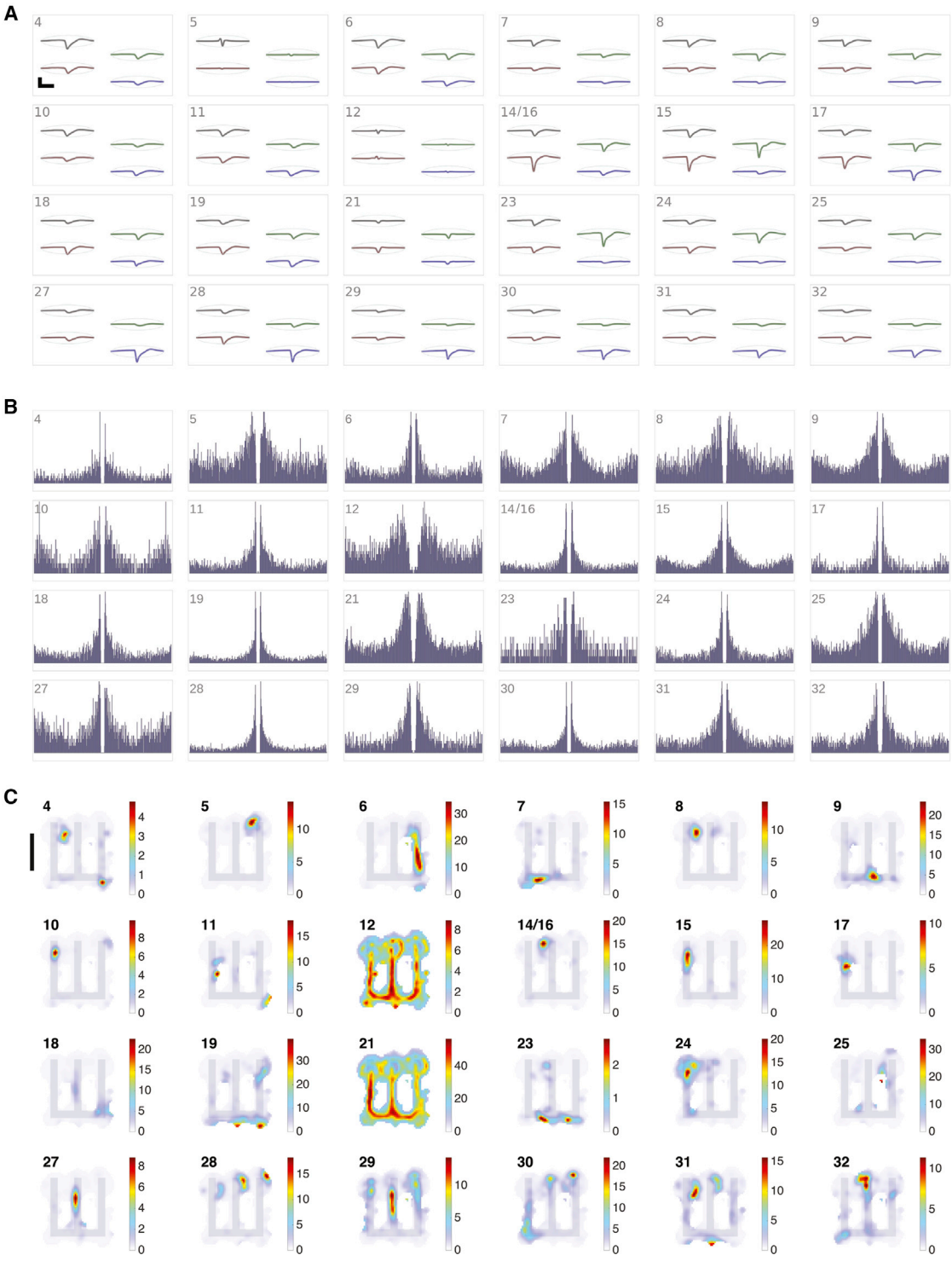

Figure 3. All MountainSort-Identified Putative Single-Unit Clusters from the Hippocampal CA1 Tetrode Dataset

(A) Average waveforms (band-pass filtered 300–6,000 Hz) for the putative single-unit clusters as determined using metric thresholds: noise overlap <0.03, isolation >0.95, firing rate >0.05 Hz. MountainSort cluster ID is inset. Scale, 250 μv and 1 ms.

(B) Autocorrelograms for the corresponding clusters; x axis range is ± 100 ms, normalized y axis range.

(C) Occupancy-normalized spatial firing rate maps for the inset MountainSort cluster ID. Track outline is shown in gray. Scale bar, 50 cm.

This was MountainSort cluster 21. When using a single channel instead of all four channels, we found a noise overlap of 0.052 versus 0.021, isolation 0.98 versus 0.99, and SNR 5.05 versus 3.40. Interestingly, this is an interneuron of relatively low amplitude (mean peak height of ~110 μv). This suggests that single channels are insufficient to isolate single neurons, at least in hippocampal area CA1. We believe this would be true for any sorting algorithm.

Sorting of Multi-contact Electrode Arrays

While tetrodes remain in use across many laboratories, new, high-density multielectrode arrays offer the ability to record from much larger ensembles of neurons (Berényi et al., 2014; Du et al., 2011; Rios et al., 2016). MountainSort has a number of features designed specifically for such arrays. To demonstrate and evaluate these features, we applied our algorithm to 7 hr of data from a 16-channel, polymer probe (Figure 4A) (Tooker et al., 2013, 2014) dataset with challenges similar to those of the tetrode dataset used in Figures 2 and 3. Although this array was placed in a different brain region (prelimbic cortex), had four times as many channels as the tetrode recording shown above, and contained a full 7 hr of continuous recording, we used identical parameters for the clustering pipeline and for the quality metric thresholds.

Recall that MountainSort independently applies spike sorting on small electrode neighborhoods and then consolidates across all channels. In the case of the 16-channel probe, each local neighborhood consisted of up to seven electrodes. As a consequence, the feature space in which each electrode's clustering was done was derived from a different, sometimes non-overlapping, set of electrodes. This is a notable difference with the tetrode dataset where every channel was included in every neighborhood.

Applying MountainSort to this dataset resulted in the identification of 37 putative single units (Figure 4B). Importantly, as in Figure 3, the putative single units have few, if any, refractory period violations (Figure 4C). Putative noise clusters (noise overlap >0.03) are shown in Figure S4. After removing clusters with high noise overlap, there was only one cluster pair flagged as non-isolated (isolation <0.95). This was the one identified bursting cell pair, MountainSort ID 32 and 33, 0.91 isolation (Figure S4C). The cluster pair with the next highest overlap was cluster pair 30 and 31, 0.97 isolation, a pair identified as putative single units during automated annotation (Figure S4D). These results demonstrate that MountainSort can be applied to a range of datasets without the need for parameter adjustments.

Comparison with Other Sorting Algorithms

MountainSort aims to provide a fully automated spike sorting pipeline in the sense that it takes as input a raw time series and generates a set of well-isolated clusters. Most other software packages provide only a degree of automation by producing a set of clusters requiring further curation. This is oftentimes done using manual means: the expectation is that users will discard, merge, and sometimes even split clusters before using the results for downstream analyses. Setting aside the issue of human intervention, we compared MountainSort with two other spike sorting packages: KiloSort (Pachitariu et al., 2016) and Spyking Circus (Yger et al., 2016). The three algorithms were applied to (1) real data from our laboratory (the tetrode dataset described above), (2) a publicly available extracellular dataset with known ground truth (128-channel silicon polytrode together with a juxtacellular ground-truth measurement) (Neto et al., 2016), and (3) simulated data obtained from superimposing synthetic waveforms on background signal taken from a real dataset. Each of the three software packages has parameters that can be modified to optimize performance for different applications. However, as our objective is to create a spike sorting environment that is well suited to a diverse set of problems without requiring parameter tuning, we used the recommended set of parameters in each of the three packages (i.e., default values or the settings used in the examples distributed with the software). Importantly, for each algorithm we used the same parameters in all three experimental settings.

Confusion matrices comparing MountainSort with KiloSort and Spyking Circus on the hippocampal dataset are shown in Figure 5. For visualization purposes, the obviously invalid clusters (based on autocorrelograms) were manually excluded from KiloSort and Spyking Circus prior to assembling the matrices. These matrices make it clear that the three algorithms find many of the same units but also highlight a number of clusters where the algorithms produce different results. These include one cluster that MountainSort identified but KiloSort did not (MountainSort 12) and nine clusters that MountainSort identified but KiloSort merged into other clusters (MountainSort 18, 7, 23, 25, 29, 11, 10, 27, 17), seven clusters that MountainSort identified but Spyking Circus did not (MountainSort 5, 27, 25, 12, 9, 8, 7), and seven clusters that MountainSort identified but Spyking Circus merged into other clusters (MountainSort 10, 23, 18, 17, 16, 11, 4). Taken together, neither KiloSort nor Spyking Circus identified MountainSort 12, and both KiloSort and Spyking Circus merged MountainSort 18, 17, 11, 10, and 23 into other clusters. The seven clusters found by KiloSort but not by MountainSort (appearing on the right side of Figure 5A) correspond to low-amplitude clusters rejected in the automated annotation stage of MountainSort for having a high noise overlap score.

Based on autocorrelograms and place maps, we believe the clusters found by MountainSort and not by the other algorithms to be valid units, including MountainSort 12, a putative interneuron. Clusters in the KiloSort or Spyking Circus sorting that comprise events from multiple MountainSort clusters (Figure 5) could be the result of a MountainSort false split or a KiloSort or Spyking Circus false merge. For simplicity, attention was focused on the cases where KiloSort and Spyking Circus had the same or overlapping MountainSort cluster subsets (KiloSort 48, Spyking Circus 6; KiloSort 8, Spyking Circus 23; KiloSort 2, Spyking Circus 2). Despite KiloSort and Spyking Circus having a degree of agreement, the MountainSort clusters showed appreciable differences in PC analysis (PCA) projections, waveforms, and spatial firing properties (Figure S5), suggesting that the MountainSort clusters were more likely to correspond to well-isolated single units.

We then applied MountainSort, KiloSort, and Spyking Circus to a publicly available 128-channel dataset with independent juxtacellular firing information for one of the cells (Neto et al., 2016).

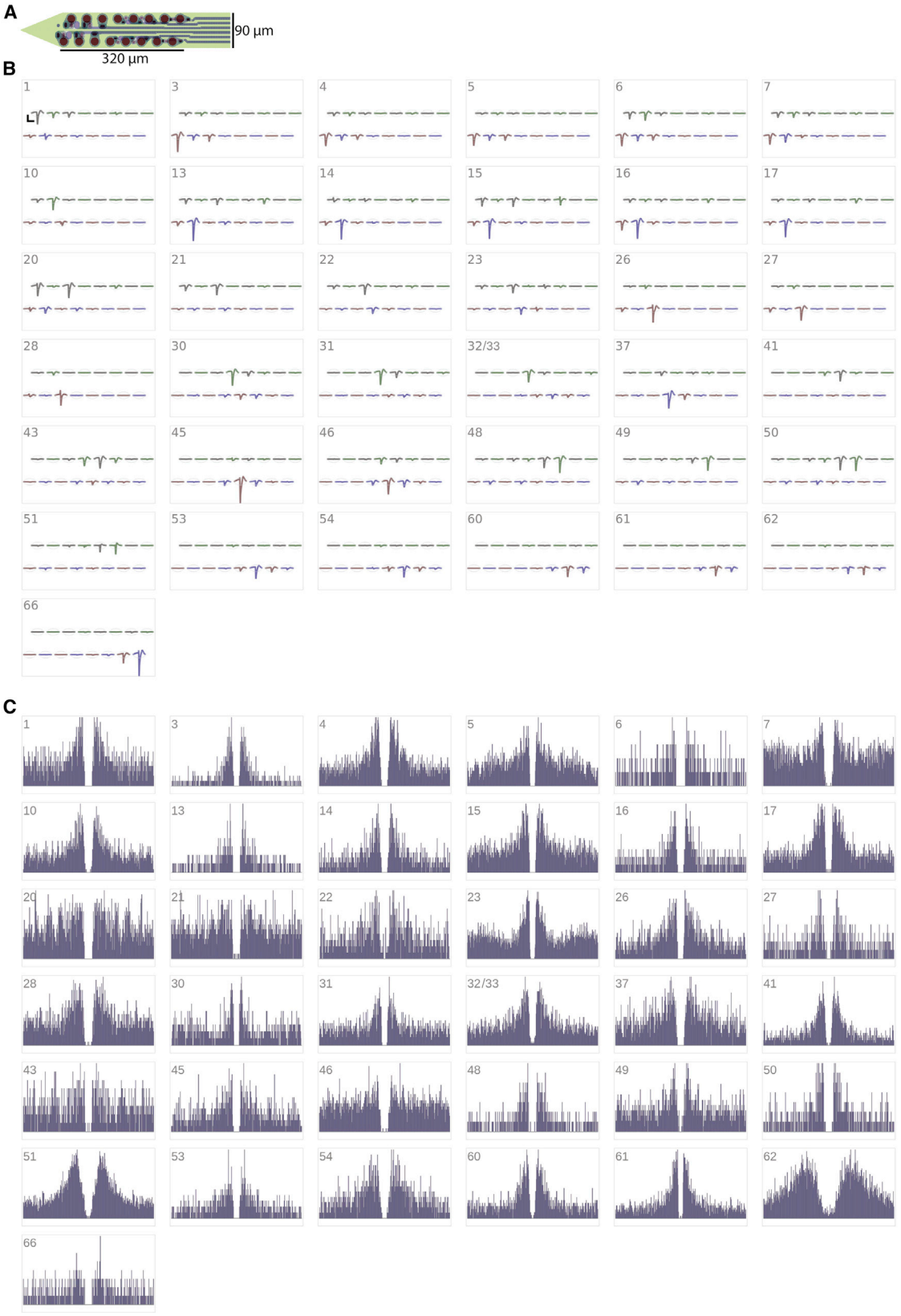

(legend on next page)

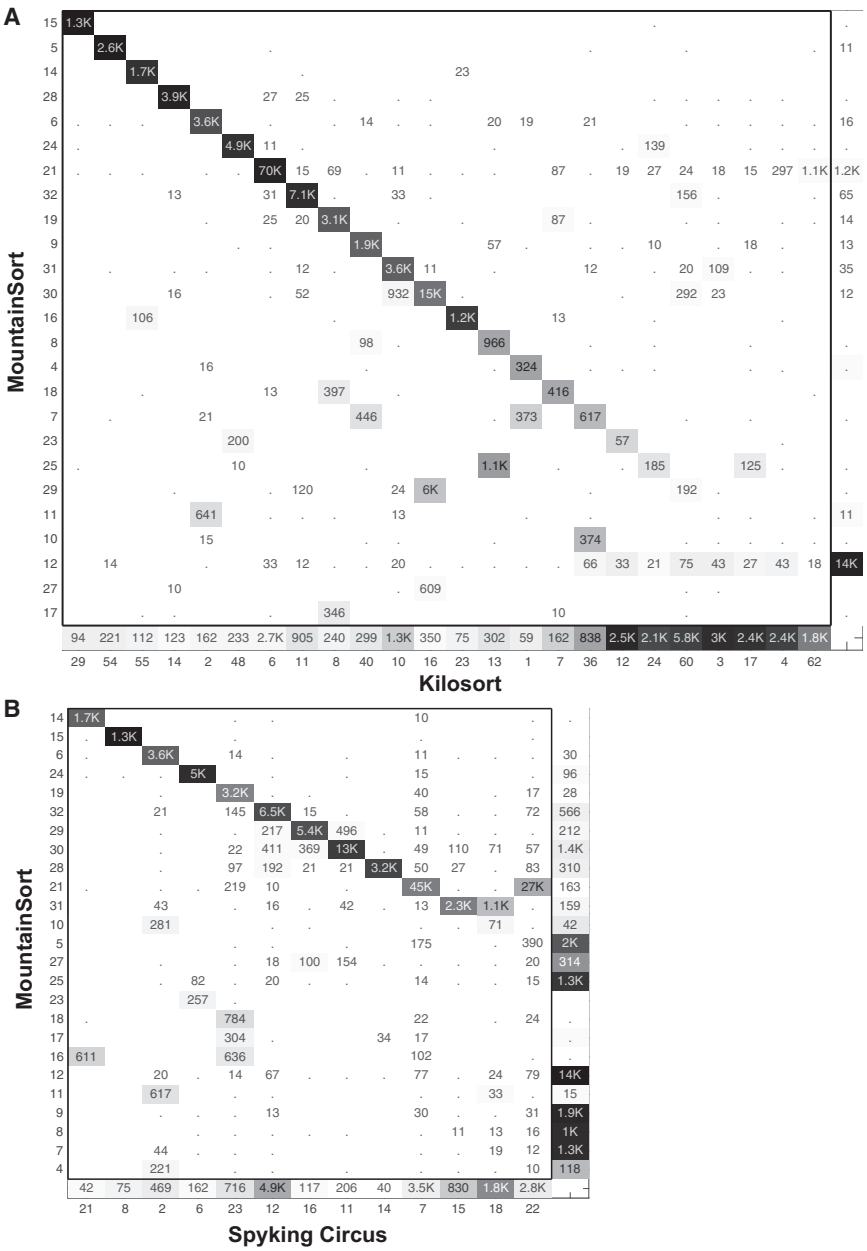

Figure 5. Confusion Matrices Comparing MountainSort with Kilosort and Spyking Circus Applied to the Hippocampal Tetrode Dataset of Figure 3

The comparison to Kilosort is shown in (A), and the comparison to Spyking Circus is shown in (B). See Figure S2 for details on interpreting confusion matrices. For readability, entries with fewer than ten events are marked with a period. MountainSort is fully automated, whereas a number of obviously invalid clusters needed to be manually excluded from the KiloSort and Spyking Circus runs before assembling the confusion matrix.

This dataset is one of ten datasets in the repository exhibiting varying levels of sorting difficulty. We found that only one of these featured a (ground-truthed) cell with sufficiently high amplitude-to-noise ratio to perform accurate sorting using any of the techniques. MountainSort identified this high amplitude unit with very high accuracy (>99%; 24 false-positives and 32 false-negatives out of 4,895 true events) and appropriately marked it as a bursting pair. KiloSort also split the unit into two pieces with >99% accuracy, but has no mechanism to report bursting pairs. Spyking Circus split the true cluster into two pieces, but the larger portion (60% of events) were merged with a low-amplitude cluster that included many false-positives. Instructions for running these algorithms on this publicly available dataset are provided in the software repository for MountainSort.

In addition, we applied the algorithms to a publicly available tetrode recording from a rat hippocampus (Harris et al., 2000) with a juxtacellular ground truth channel. MountainSort found the unit with 10% false-positives and 11% false-negatives. Spyking Circus had only 6% false-positives but 21% false-negatives. KiloSort could not be run (in the current version of the software) because the channel count was too low.

Figure 6 shows that MountainSort has a consistently higher accuracy score than the other two algorithms, particularly when the number of detectable clusters is high (Figure 6C). We note, however, that because we chose the default/recommended parameters for the three algorithms, these results do not preclude the possibility that KiloSort and Spyking Circus could do better if parameters were adjusted.

Assessment of Computational Efficiency

MountainSort was also able to cluster all of these datasets much faster than real time. We carried out timing tests on a Linux workstation with 192 GB RAM and 20 physical processors with

Figure 4. MountainSort Identification of Well-Isolated Units for 16-Channel Probe

(A) Geometric layout of polymer probe. Contact size 20 μm, horizontal contact edge-to-edge 20 μm, vertical contact edge-to-edge 38 μm.

(B) Average waveforms filtered 300–6,000 Hz, of putative single units with waveforms organized according to (A), with cluster identification number inset. Scale bar, 100 μv and 2 ms.

(C) Corresponding autocorrelograms. x axis scale 100 ms, normalized y axis scale.

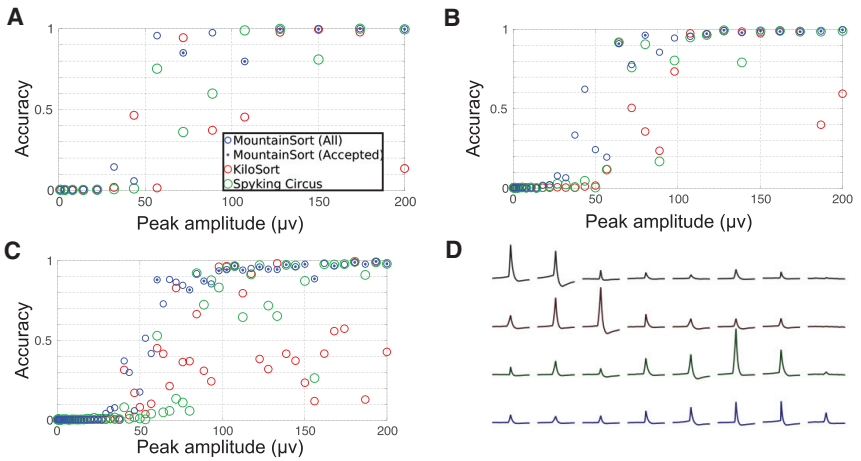

Figure 6. Comparison among MountainSort, KiloSort, and Spyking Circus Using Three Simulated Datasets

(A–C) Synthetically generated spike waveforms were superimposed at random times on background signal taken from a real dataset (see STAR Methods). Accuracies for each simulated cluster (see STAR Methods) are plotted against the peak amplitude of the waveform. Clusters not matching any true units are not shown. Clusters automatically accepted by MountainSort (using the isolation and noise overlap metrics) are marked using a filled-in blue circle.

(D) Synthetic waveforms for the eight clusters with largest peak amplitudes in the simulated dataset shown in (A).

hyper-threading capability (although not all cores were used in the experiments, as indicated). The 46-min, four-channel dataset used in Figures 2 and 3 had a total MountainSort runtime of 40 s (including 22 s preprocessing) when run using 16 threads. This is around 70 times faster than real time. The 6.6 hr, 16-channel dataset used in Figure 4 involved over 7 million detected events and had a total MountainSort runtime of 805 s (including 336 s preprocessing) using 16 threads. This is 30 times real time. The 128-channel publicly available dataset with juxtacellular ground truth (Neto et al., 2016) was sorted in 249 s (including 128 s preprocessing) using 40 threads. This represents 2.5 times real time.

To assess how processing times scale with the duration of recording and number of events, we processed subsets of the 7 hr, 16-channel probe dataset that contained ~1.1 million events per hour. We found that processing times scaled roughly linearly with the data duration, with a preprocessing time of ~1 min per hour of the recording and a sorting time of ~1.3 min per hour (Figure 7A). We also wanted to assess the efficiency on machines with fewer processing cores. We varied the number of logical cores between four and 20 for processing a 4-hr subset of the same 16-channel data. We note that, even though the processing is fastest when using 16 or more threads, the processing speed is still much faster than real time when restricting to only four logical cores. Taken together, and even assuming linear scaling with the number of electrodes (sublinear scaling is expected due to parallelization if we also increase the number of cores), our results suggest that 320 channels from the same electrode array could be sorted in real time on a single machine; this is on the order of the graphical processing unit (GPU) rate reported in Pachitariu et al. (2016) for KiloSort.

DISCUSSION

The MountainSort software suite provides fully automated spike sorting from electrode arrays of varied sizes and geometries in multiple brain regions, with accuracies comparable to or exceeding existing standards, and computational times much faster than acquisition times on non-specialized hardware. Importantly, MountainSort is also a fully functional package providing an intuitive graphical user interface with the ability to visualize subsets of selected clusters and annotation tools for exporting the data (see the online source code repository for documentation and tutorials). This stands in contrast to many previously developed clustering algorithms, where it would be difficult for users to test out algorithms on their own data. Thus, it is relatively straightforward to incorporate MountainSort into a laboratory's data processing pipeline.

To our knowledge, this is the first time that a fully automated spike sorting approach has been demonstrated to have comparable error rates to existing manual and semi-manual standards. Moreover, MountainSort sorted a dataset from the hippocampus better than humans, despite the presence of both complex spike bursts and noise events that arise from muscle and movement-related artifacts. Indeed, MountainSort identified many more putative single units from a hippocampal CA1 tetrode than manual sorters (24 versus 5–10). We note here that there are principled reasons to expect that MountainSort would outperform manual sorting. Typical manual sorting, such as in this study, is done in a static feature space of four to 16 dimensions (such as amplitude on channel 1, peak-to-trough ratio on channel 3, etc.), computed from filtered waveforms. Moreover, manual sorting usually involves drawing polygons in two dimensional projections. In contrast, MountainSort operates in a ten-dimensional space corresponding to the first ten PCs, computed from spatially whitened waveforms (effectively it is more than ten dimensions when considering the branch method, see STAR Methods). Moreover, each of the ten dimensions does not correspond to only one channel at a time, as with some other clustering approaches, but instead each is a PC across all of the channels of the neighborhood. Further aiding in separation is the recomputation of the PCs when doing cluster comparisons. Due to these differences, it is highly likely that MountainSort can more reliably separate clusters than could a human operator, the current gold standard for tetrode spike sorting.

Comparison of MountainSort to two other recently released packages, KiloSort and Spyking Circus, suggests that MountainSort also performs better than these other packages. When applied to the hippocampal dataset, all three algorithms identified a subset of well-isolated units, but MountainSort found units that were not identified by Spyking Circus, and both

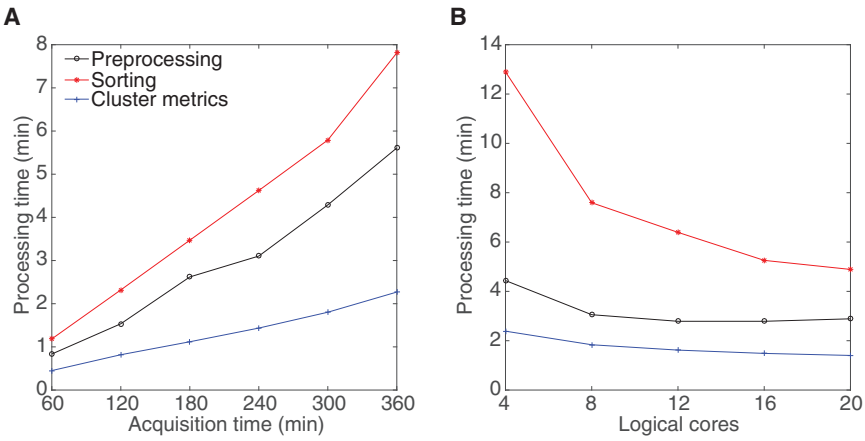

Figure 7. Computational Efficiency by Processing Stage

All plots are from the 16-channel polymer probe dataset from Figure 4.

(A) Processing time versus acquisition time. Each hour of recording contains about 2 million events.

(B) Processing time versus number of logical cores used (i.e., processing threads).

KiloSort and Spyking Circus merged units with distinct PCA features and spatial firing patterns that MountainSort separated. Comparisons on simulated data revealed the same trends: MountainSort consistently identified units with greater accuracy than the other algorithms.

These comparisons highlight two other features of MountainSort. First, these comparisons were based on using the default parameter values for all three algorithms. While it is possible that different parameters could have improved the performance of KiloSort and Spyking Circus, one of our major goals was to develop an algorithm with essentially no free parameters, and our success in sorting data from multiple brain regions as well as multiple simulated dataset using the same parameters illustrates the power of this approach. Second, while these comparisons used the fully automated output from MountainSort, manual curation remained necessary for both KiloSort and Spyking Circus. It is important to note that these algorithms were not designed to be fully automatic, so the need for manual curation is not surprising, but it remains the case that, at the time of this publication, only MountainSort is successful in a fully automated mode.

Automation provides clear benefits for reproducibility among sortings of the same data and comparability across datasets. This is accomplished using novel isolation and noise overlap metrics. By contrast, commonly used cluster metrics, such as isolation distance (Harris et al., 2001) and L-ratio (Schmitzer-Torbert et al., 2005; Schmitzer-Torbert and Redish, 2004), utilize Mahalanobis distance calculations, which are dependent upon the dimensionality of the selected feature space, making it difficult to compare cluster quality between datasets. Furthermore, the commonly used L-ratio metric, among others (Hill et al., 2011), makes the assumption of a multivariate normal cluster distributions, which can be problematic because this is often not valid as in cases of burst firing or electrode drift. By taking into account dataset-specific noise and nearest neighbor distances, our noise overlap and isolation metrics provide a nonparametric means to compare cluster quality across datasets.

This ability to compare quality across datasets allow these cluster quality metrics, combined with the annotation and provenance strategy built in to MountainSort, to be propagated to downstream analyses. Maintaining access to all clusters and their cluster quality metrics, including those that likely correspond to multiunit spiking, has a number of important advantages. First, thresholds could be established by examining how known properties of a given set of units (such as the number and size of hippocampal place fields) vary as a function of cluster quality (Harris et al., 2016). Second, simple changes in inclusion thresholds can be used for direct assessment of whether cluster quality influences a specific finding. Cluster quality could also be used to weight the contribution of each unit to a given analysis, thereby ensuring that the best isolated clusters have a proportionally greater influence on the findings. Third, there are cases where including multiunit spiking improves the quality of the results, as is the case for clusterless decoding of animal position from unsorted hippocampal spiking activity (Deng et al., 2015; Kloosterman et al., 2014). Inclusion of all clusters regardless of quality, greatly simplifies the application of these techniques to the data.

The combination of automation with a minimal set of parameters and model independence also has particular advantages. Existing spike sorting pipelines (Hill et al., 2011; Kadir et al., 2014; Pachitariu et al., 2016; Rossant et al., 2016; Yger et al., 2016) typically depend upon numerous adjustable parameters and operator judgment and even allow for cluster boundaries to be redrawn, significantly increasing potential inter-operator variability. Automation that relies on a single, common set of parameters eliminates these issues. Further, our algorithm is also effectively model-free, making only the assumption that clusters have unimodal density projections. In contrast, existing sorting algorithms that rely on a template matching step (Franke et al., 2015; Vargas-Irwin and Donoghue, 2007; Zhang et al., 2004) (i.e., minimizing the L2-norm of the error for a given model) implicitly assume a multivariate Gaussian noise model, resulting in increased variability in output and operator curation when this assumption is not valid. MountainSort's model independence offers versatility, allowing it to deal gracefully with non-Gaussian waveform variation and to be used across recording conditions and locations.

While MountainSort's assumption of unimodality works well even in the case of the hippocampal cells (with non-Gaussian cluster distributions) we applied it to, there are still cases where bursting results in multiple unimodal clusters that should be merged. MountainSort therefore involves a post-processing step for automatically detecting clusters that are bursting pairs. The software also provides annotation tools to allow the user to indicate that he or she believes that the clusters should be

merged, but importantly the original automatic clustering is also preserved in the sorting output, allowing for identification of all user decisions. This occasional need for manual merging could be further mitigated by using additional post-clustering analyses beyond our current relatively simple automated bursting pair criteria (Harris et al., 2001; Quirk et al., 2001; Quirk and Wilson, 1999).

MountainSort also runs quickly, even on large datasets. Clustering is always performed on local electrode neighborhoods, so clustering time theoretically scales linearly with the number of channels. Importantly, the clustering stage, along with most other stages of the processing, is implemented as parallel computations that can be run simultaneously on multiple central processing unit (CPU) cores. As a result, the total time required for sorting and metric computation was much shorter than the recording times for the same data on standard computer hardware for both tetrodes (70× real time) and a 16-channel polymer probe (30× real time). These speed-ups are in line with other approaches (Pachitariu et al., 2016; Yger et al., 2016) where strategies such as hardware acceleration have brought computational times down significantly. However, these alternative approaches lack an automated curation component. As computers become increasingly powerful, the time spent by manual operators remains the largest bottleneck to spike sorting. With the elimination of manual curation, total sorting time becomes faster than acquisition time, and we can explore further directions that would otherwise be infeasible. One is the ability to run the clustering algorithm multiple times, allowing for cross-validation in the absence of ground truth (Barnett et al., 2016). Such stability metrics ensure that clustering results are not overly sensitive to realistic noise perturbations.

While MountainSort offers substantial advantages over current manual and semi-automatic clustering methods, additional work will be required to fully address two remaining challenges: overlapping spikes and drift. Currently, as with KlustaKwik (Kadir et al., 2014; Rossant et al., 2016), it has no problem with coincident spiking events where the two neurons are sufficiently separated in space (i.e., induce peak signal on different channels). However, neither package solves the harder problem of resolving spike waveforms that significantly overlap on the same electrode. Current solutions to that problem rely on model-based frameworks (Ekanadham et al., 2014; Franke et al., 2010; Pachitariu et al., 2016; Pillow et al., 2013), which, as discussed, include strong noise model assumptions. These approaches have been shown to be successful when applied to in vitro datasets, and it may be possible to adapt these approaches as a post-sorting step to identify events that are best explained as the superposition of two or more spikes.

MountainSort naturally handles some level of drift, where there are systematic changes in waveforms thought to result from movement of electrodes relative to the tissue or perhaps due to glial cells migrating along electrode shanks (Bar-Hillel et al., 2006; Calabrese and Paninski, 2011; Chestek et al., 2007; Emondi et al., 2004). We expect that MountainSort will correctly identify cluster boundaries as long as the resultant time-collapsed cluster is unimodal and does not overlap with another cluster. Errors are expected when these time-collapsed clusters overlap with one another, however. That said, because MountainSort can be run on overlapping sections of data, it is conceptually straightforward to include augmentations that link clusters across time slices using segmentation fusion based algorithms (Dhawale et al., 2015). Cases where clusters drift in and out of noise or other clusters are more problematic, both for MountainSort and for all other current approaches. Here, the new cluster metrics we have developed can be helpful, as clusters that drift into other clusters or the noise will tend to have poor isolation and noise overlap scores, allowing identification of times the cluster is sufficiently uncontaminated.

Taken together, our findings demonstrate that MountainSort is a sensible and efficient automated solution to the spike sorting problem. With a combination of minimal assumptions, fast run times, and a powerful graphical user interface, MountainSort can greatly shorten the time required for spike sorting while increasing the reproducibility and transparency of the process. With one electrode channel neighborhood allocated per available logical core, MountainSort is naturally extensible to distributed computing and large electrode arrays. Our approach is compatible with future refinements and extensions for resolving overlapping spikes and tracking units in the presence of drift.

STAR★METHODS

Detailed methods are provided in the online version of this paper and include the following:

- KEY RESOURCES TABLE
- CONTACT FOR REAGENT AND RESOURCE SHARING
- EXPERIMENTAL MODEL AND SUBJECT DETAILS
  - Rat
- METHOD DETAILS
  - Filtering and Spatial Whitening
  - Event Detection
  - Feature Extraction and the Branch Method
  - Clustering via ISO-SPLIT
  - ISO-CUT
  - Cluster Consolidation across Electrodes
- ELIMINATING REDUNDANT EVENTS VIA FITTING
  - Isolation and Noise Overlap Metrics
  - Automatic Identification of Bursting Clusters
  - Manual Clustering
  - Simulations Using Synthetic Data
  - Computational Efficiency Measurements
  - In Vivo Datasets
- DATA AND SOFTWARE AVAILABILITY

SUPPLEMENTAL INFORMATION

Supplemental Information includes five figures and can be found with this article online at http://dx.doi.org/10.1016/j.neuron.2017.08.030.

AUTHOR CONTRIBUTIONS

J.F.M., A.H.B., and L.F.G. developed the methodology. J.F.M. and A.H.B. wrote the software. J.E.C. collected and curated tetrode and polymer probe datasets. J.F.M., J.E.C., and A.H.B. analyzed the data. V.M.T., A.C.T., K.Y.L., K.G.S., and S.H.F. developed and fabricated the polymer probes. J.F.M., J.E.C., A.H.B., L.M.F., and L.F.G. conceptualized the project and wrote the manuscript.

ACKNOWLEDGMENTS

The Flatiron Institute is a division of the Simons Foundation. This work was also supported by NINDS grant U01NS090537 to L.M.F. and V.M.T. and NIMH grant F30MH109292 to J.E.C. We thank Kevin Fan for assistance with data collection, Demetris Roumis and Marielena Sosa for manual clustering, and Witold Wysota for programming support. We are grateful for helpful discussions with E.J. Chichilnisky, Eero Simoncelli, György Buzsáki, Adrien Peyrache, Carl Schoonover, and Andrew Fink.

Received: December 27, 2016
Revised: July 6, 2017
Accepted: August 16, 2017
Published: September 13, 2017

REFERENCES

Abeles, M., and Goldstein, M.H. (1977). Multispike train analysis. Proc. IEEE *65*, 762–773.

Bar-Hillel, A., Spiro, A., and Stark, E. (2006). Spike sorting: Bayesian clustering of non-stationary data. J. Neurosci. Methods *157*, 303–316.

Barnett, A.H., Magland, J.F., and Greengard, L.F. (2016). Validation of neural spike sorting algorithms without ground-truth information. J. Neurosci. Methods *264*, 65–77.

Berényi, A., Somogyvári, Z., Nagy, A.J., Roux, L., Long, J.D., Fujisawa, S., Stark, E., Leonardo, A., Harris, T.D., and Buzsáki, G. (2014). Large-scale, high-density (up to 512 channels) recording of local circuits in behaving animals. J. Neurophysiol. *111*, 1132–1149.

Calabrese, A., and Paninski, L. (2011). Kalman filter mixture model for spike sorting of non-stationary data. J. Neurosci. Methods *196*, 159–169.

Carlson, D.E., Vogelstein, J.T., Qisong Wu, Wenzhao Lian, Mingyuan Zhou, Stoetzner, C.R., Kipke, D., Weber, D., Dunson, D.B., and Carin, L. (2014). Multichannel electrophysiological spike sorting via joint dictionary learning and mixture modeling. IEEE Trans. Biomed. Eng. *61*, 41–54.

Chestek, C.A., Batista, A.P., Santhanam, G., Yu, B.M., Afshar, A., Cunningham, J.P., Gilja, V., Ryu, S.I., Churchland, M.M., and Shenoy, K.V. (2007). Single-neuron stability during repeated reaching in macaque premotor cortex. J. Neurosci. *27*, 10742–10750.

Csicsvari, J., Henze, D.A., Jamieson, B., Harris, K.D., Sirota, A., Barthó, P., Wise, K.D., and Buzsáki, G. (2003). Massively parallel recording of unit and local field potentials with silicon-based electrodes. J. Neurophysiol. *90*, 1314–1323.

Deng, X., Liu, D.F., Kay, K., Frank, L.M., and Eden, U.T. (2015). Clusterless decoding of position from multiunit activity using a marked point process filter. Neural Comput. *27*, 1438–1460.

Dhawale, A.K., Poddarr, R., Kopelowitz, E., Normand, V., Wolff, S., and Olveczky, B. (2015). Automated long-term recording and analysis of neural activity in behaving animals. bioRxiv. http://dx.doi.org/10.1101/033266.

Du, J., Blanche, T.J., Harrison, R.R., Lester, H.A., and Masmanidis, S.C. (2011). Multiplexed, high density electrophysiology with nanofabricated neural probes. PLoS ONE *6*, e26204.

Einevoll, G.T., Franke, F., Hagen, E., Pouzat, C., and Harris, K.D. (2012). Towards reliable spike-train recordings from thousands of neurons with multielectrodes. Curr. Opin. Neurobiol. *22*, 11–17.

Ekanadham, C., Tranchina, D., and Simoncelli, E.P. (2014). A unified framework and method for automatic neural spike identification. J. Neurosci. Methods *222*, 47–55.

Emondi, A.A., Rebrik, S.P., Kurgansky, A.V., and Miller, K.D. (2004). Tracking neurons recorded from tetrodes across time. J. Neurosci. Methods *135*, 95–105.

Fee, M.S., Mitra, P.P., and Kleinfeld, D. (1996). Automatic sorting of multiple unit neuronal signals in the presence of anisotropic and non-Gaussian variability. J. Neurosci. Methods *69*, 175–188.

Frank, L.M., Brown, E.N., and Wilson, M. (2000). Trajectory encoding in the hippocampus and entorhinal cortex. Neuron *27*, 169–178.

Frank, L.M., Stanley, G.B., and Brown, E.N. (2004). Hippocampal plasticity across multiple days of exposure to novel environments. J. Neurosci. *24*, 7681–7689.

Franke, F., Natora, M., Boucsein, C., Munk, M.H.J., and Obermayer, K. (2010). An online spike detection and spike classification algorithm capable of instantaneous resolution of overlapping spikes. J. Comput. Neurosci. *29*, 127–148.

Franke, F., Quian Quiroga, R., Hierlemann, A., and Obermayer, K. (2015). Bayes optimal template matching for spike sorting - combining fisher discriminant analysis with optimal filtering. J. Comput. Neurosci. *38*, 439–459.

Freund, T.F., and Buzsáki, G. (1996). Interneurons of the hippocampus. Hippocampus *6*, 347–470.

Gray, C.M., Maldonado, P.E., Wilson, M., and McNaughton, B. (1995). Tetrodes markedly improve the reliability and yield of multiple single-unit isolation from multi-unit recordings in cat striate cortex. J. Neurosci. Methods *63*, 43–54.

Harris, K.D., Henze, D.A., Csicsvari, J., Hirase, H., and Buzsáki, G. (2000). Accuracy of tetrode spike separation as determined by simultaneous intracellular and extracellular measurements. J. Neurophysiol. *84*, 401–414.

Harris, K.D., Hirase, H., Leinekugel, X., Henze, D.A., and Buzsáki, G. (2001). Temporal interaction between single spikes and complex spike bursts in hippocampal pyramidal cells. Neuron *32*, 141–149.

Harris, K.D., Quiroga, R.Q., Freeman, J., and Smith, S.L. (2016). Improving data quality in neuronal population recordings. Nat. Neurosci. *19*, 1165–1174.

Hartigan, J.A., and Hartigan, P. (1985). The dip test of unimodality. Ann. Stat. *13*, 70–84.

Hill, D.N., Mehta, S.B., and Kleinfeld, D. (2011). Quality metrics to accompany spike sorting of extracellular signals. J. Neurosci. *31*, 8699–8705.

Kadir, S.N., Goodman, D.F.M., and Harris, K.D. (2014). High-dimensional cluster analysis with the masked EM algorithm. Neural Comput. *26*, 2379–2394.

Kim, S.M., and Frank, L.M. (2009). Hippocampal lesions impair rapid learning of a continuous spatial alternation task. PLoS ONE *4*, e5494.

Kloosterman, F., Layton, S.P., Chen, Z., and Wilson, M.A. (2014). Bayesian decoding using unsorted spikes in the rat hippocampus. J. Neurophysiol. *111*, 217–227.

Kuhn, H.W. (1955). The Hungarian method for the assignment problem. Naval Research Logistics Quarterly *2*, 83–97.

Lewicki, M.S. (1998). A review of methods for spike sorting: the detection and classification of neural action potentials. Network *9*, R53–R78.

Lopez, C.M., Mitra, S., Putzeys, J., Raducanu, B., Ballini, M., Andrei, A., Severi, S., Welkenhuysen, M., Van Hoof, C., Musa, S., and Yazicioglu, R.F. (2016). A 966-electrode neural probe with 384 configurable channels in 0.13 μm SOI CMOS. 2016 IEEE International Solid-State Circuits Conference, 392–393.

Magland, J.F., and Barnett, A.H. (2016). Unimodal clustering using isotonic regression: ISO-SPLIT. arXiv, arXiv:1508.04841v2, https://arxiv.org/abs/1508.04841.

Marre, O., Amodei, D., Deshmukh, N., Sadeghi, K., Soo, F., Holy, T.E., and Berry, M.J., 2nd (2012). Mapping a complete neural population in the retina. J. Neurosci. *32*, 14859–14873.

Massey, F. (1951). The Kolmogorov-Smirnov test for goodness of fit. J. Am. Stat. Assoc. *46*, 68–78.

McNaughton, B.L., O'Keefe, J., and Barnes, C.A. (1983). The stereotrode: A new technique for simultaneous isolation of several single units in the central nervous system from multiple unit records. J. Neurosci. Methods *8*, 391–397.

Muller, R. (1996). A quarter of a century of place cells. Neuron *17*, 813–822.

Neto, J.P., Lopes, G., Frazão, J., Nogueira, J., Lacerda, P., Baião, P., Aarts, A., Andrei, A., Musa, S., Fortunato, E., et al. (2016). Validating silicon polytrodes with paired juxtacellular recordings: Method and dataset. J. Neurophysiol. *116*, 892–903.

O'Keefe, J., and Dostrovsky, J. (1971). The hippocampus as a spatial map. Preliminary evidence from unit activity in the freely-moving rat. Brain Res. *34*, 171–175.

Pachitariu, M., Steinmetz, N., Kadir, S., Carandini, M., and Harris, K. (2016). Kilosort: realtime spike-sorting for extracellular electrophysiology with hundreds of channels. bioRxiv. http://dx.doi.org/10.1101/061481.

Pedreira, C., Martinez, J., Ison, M.J., and Quian Quiroga, R. (2012). How many neurons can we see with current spike sorting algorithms? J. Neurosci. Methods *211*, 58–65.

Pillow, J.W., Shlens, J., Chichilnisky, E.J., and Simoncelli, E.P. (2013). A model-based spike sorting algorithm for removing correlation artifacts in multi-neuron recordings. PLoS ONE *8*, e62123.

Quirk, M.C., and Wilson, M.A. (1999). Interaction between spike waveform classification and temporal sequence detection. J. Neurosci. Methods *94*, 41–52.

Quirk, M.C., Blum, K.I., and Wilson, M.A. (2001). Experience-dependent changes in extracellular spike amplitude may reflect regulation of dendritic action potential back-propagation in rat hippocampal pyramidal cells. J. Neurosci. *21*, 240–248.

Quiroga, R.Q. (2012). Spike sorting. Curr. Biol. *22*, R45–R46.

Quiroga, R.Q., Nadasdy, Z., and Ben-Shaul, Y. (2004). Unsupervised spike detection and sorting with wavelets and superparamagnetic clustering. Neural Comput. *16*, 1661–1687.

Rios, G., Lubenov, E.V., Chi, D., Roukes, M.L., and Siapas, A.G. (2016). Nanofabricated neural probes for dense 3-D recordings of brain activity. Nano Lett. *16*, 6857–6862.

Rodriguez, A., and Laio, A. (2014). Machine learning. Clustering by fast search and find of density peaks. Science *344*, 1492–1496.

Rossant, C., Kadir, S.N., Goodman, D.F.M., Schulman, J., Hunter, M.L.D., Saleem, A.B., Grosmark, A., Belluscio, M., Denfield, G.H., Ecker, A.S., et al. (2016). Spike sorting for large, dense electrode arrays. Nat. Neurosci. *19*, 634–641.

Santhanam, G., Linderman, M.D., Gilja, V., Afshar, A., Ryu, S.I., Meng, T.H., and Shenoy, K.V. (2007). HermesB: A continuous neural recording system for freely behaving primates. IEEE Trans. Biomed. Eng. *54*, 2037–2050.

Schmitzer-Torbert, N., and Redish, A.D. (2004). Neuronal activity in the rodent dorsal striatum in sequential navigation: Separation of spatial and reward responses on the multiple T task. J. Neurophysiol. *91*, 2259–2272.

Schmitzer-Torbert, N., Jackson, J., Henze, D., Harris, K., and Redish, A.D. (2005). Quantitative measures of cluster quality for use in extracellular recordings. Neuroscience *131*, 1–11.

Shobe, J.L., Claar, L.D., Parhami, S., Bakhurin, K.I., and Masmanidis, S.C. (2015). Brain activity mapping at multiple scales with silicon microprobes containing 1,024 electrodes. J. Neurophysiol. *114*, 2043–2052.

Swindale, N.V., and Spacek, M.A. (2014). Spike sorting for polytrodes: A divide and conquer approach. Front. Syst. Neurosci. *8*, 6.

Takahahi, S., Sakurai, Y., Tsukada, M., and Anzai, Y. (2002). Classification of neuronal activities from tetrode recordings using independent component analysis. Neurocomputing *49*, 289–298.

Takekawa, T., Isomura, Y., and Fukai, T. (2012). Spike sorting of heterogeneous neuron types by multimodality-weighted PCA and explicit robust variational Bayes. Front. Neuroinform. *6*, 5.

Tooker, A., Tolosa, V., Shah, K., Sheth, H., Felix, S., Delima, T., and Pannu, S. (2013). Optimization of multi-layer metal neural probe design. In 34th Annual International Conference of the IEEE EMBS (San Diego, CA).

Tooker, A., Liu, D., Anderson, E.B., Felix, S., Shah, K.G., Lee, K.Y., Chung, J.E., Pannu, S., Frank, L., and Tolosa, V. (2014). Towards a large-scale recording system: Demonstration of polymer-based penetrating array for chronic neural recording. Conf. Proc. IEEE Eng. Med. Biol. Soc. *2014*, 6830–6833.

Vargas-Irwin, C., and Donoghue, J.P. (2007). Automated spike sorting using density grid contour clustering and subtractive waveform decomposition. J. Neurosci. Methods *164*, 1–18.

Wilson, M.A., and McNaughton, B.L. (1993). Dynamics of the hippocampal ensemble code for space. Science *261*, 1055–1058.

Wood, F., Black, M.J., Vargas-Irwin, C., Fellows, M., and Donoghue, J.P. (2004). On the variability of manual spike sorting. IEEE Trans. Biomed. Eng. *51*, 912–918.

Yger, P., Spampinato, G., Esposito, E., Lefebvre, B., Deny, S., Gardella, C., Stimberg, M., Jetter, F., Zeck, G., Picaud, S., et al. (2016). Fast and accurate spike sorting in vitro and in vivo for up to thousands of electrodes. bioRxiv. http://dx.doi.org/10.1101/067843.

Zaki, M.J., and Meira, W.J. (2014). Data Mining and Analysis: Fundamental Concepts and Algorithms (Cambridge University Press).

Zhang, P.M., Wu, J.Y., Zhou, Y., Liang, P.J., and Yuan, J.Q. (2004). Spike sorting based on automatic template reconstruction with a partial solution to the overlapping problem. J. Neurosci. Methods *135*, 55–65.

STAR★METHODS

KEY RESOURCES TABLE

REAGENT or RESOURCE	SOURCE	IDENTIFIER
Deposited Data		
Ground truth rat hippocampal data	Harris et al., 2000	https://crcns.org/data-sets/hc/hc-1, d533101
Ground truth 128-ch probe data	Neto et al., 2016	http://www.kampff-lab.org/validating-electrodes/, 2015_09_03_Cell.9.0
Rat hippocampal data	This paper	http://dx.doi.org/10.17632/kmmndvycx8.1
Rat polymer probe data, part 1	This paper	http://dx.doi.org/10.17632/j2mfvnsz2t.1
Rat polymer probe data, part 2	This paper	http://dx.doi.org/10.17632/ssb8s4766s.1
Rat polymer probe data, part 3	This paper	http://dx.doi.org/10.17632/9mgpgn7fsw.1
Software and Algorithms		
MountainSort	This paper	https://github.com/magland/mountainlab
Kilosort	Pachitariu et al., 2016	https://github.com/cortex-lab/KiloSort, Commit 786584e431f01eaa08b3f09b5de2e1c3496ec16b (February 2017)
Spyking Circus	Yger et al., 2016	https://github.com/spyking-circus/spyking-circus, V0.5
MATLAB 2015b	MathWorks	https://www.mathworks.com
Trodes	SpikeGadgets	http://www.spikegadgets.com
Matclust	Mattias Karlsson	https://www.mathworks.com/matlabcentral/fileexchange/39663-matclust, V1.7
Other		
Electrophysiologic data acquisition system	SpikeGadgets	http://www.spikegadgets.com

CONTACT FOR REAGENT AND RESOURCE SHARING

Further information and requests for resources will be fulfilled by the lead contact, Loren Frank (loren@phy.ucsf.edu).

EXPERIMENTAL MODEL AND SUBJECT DETAILS

Rat

All experiments were conducted in accordance with University of California San Francisco Institutional Animal Care and Use Committee and US National Institutes of Health guidelines. Both tetrode and 16-channel probe datasets were collected from a male long-evans rat (RRID: RGD_2308852), roughly 2 months after implantation of tetrode microdrive and polymer multielectrode arrays. At the time of data collection, the rat was ~8 months of age weighing ~525 g, and was fed standard rat chow (LabDiet 5001) in addition to sweetened evaporated milk for reward during behavioral performance. The rat was ordered from Charles River Laboratories at a weight of 350 g and ~3 months of age.

METHOD DETAILS

Throughout our sorting pipeline (Figure S1A) we adhere to the objective of minimizing the number of parameters and the number of assumptions made. We also aim for full automation.

For preprocessing we used a bandpass filter implemented via Fast Fourier Transform (FFT) convolution followed by a heuristic procedure for masking out high voltage artifacts: we simply removed chunks of data with amplitudes outside of the expected range by replacing these data by zeros. We then applied a (nonparametric) spatial whitening filter to the entire time series matrix (details below) which we found to be crucial for separating nearby clusters. Both procedures where parallelized by dividing the dataset into time chunks (overlapping chunks in the case of the bandpass filter).

Sorting is initially performed separately on neighborhoods (one for each electrode channel) using information only from the central electrode and its neighbors (Figure S1B). The neighborhood patch is determined by the geometric layout and a single user-specified distance parameter, an electrode adjacency radius. For the tetrode dataset, the neighborhood comprised all four channels, but the sorting was still performed four times, with each channel being considered as the central channel on its respective local sorting. In

other words, sorting was done four times in a feature space derived from all four channels, each time only with the events detected on one of the four channels. For the 16-channel probe, neighborhoods of size 6-7 were used for all but two channels. The feature space for each electrode's sorting was derived from a different electrode neighborhood, an important difference from the tetrode dataset. The local sorting steps are event detection, clustering, and fitting as described below. In general, using larger electrode neighborhoods increases computation time, and we have observed that using more than 6-10 electrodes per neighborhood does not substantially influence sorting results for these examples.

In a second pass, the local sorting results are consolidated across electrodes to resolve duplications. By removing redundancies rather than merging clusters, we avoid a host of problematic scenarios. This is described in more detail below. Finally, per-cluster metrics are computed and automated annotation is applied so that clusters are labeled as "single unit," "noise," and "non-isolated."

Filtering and Spatial Whitening

We bandpass filter (600 Hz to 6000 Hz) each channel in a standard fashion via the FFT applied to overlapping chunks of time. As the final stage of preprocessing, spatial whitening removes correlations among channels that are not due to the neuronal signals of interest. We have found this to be crucial in separating nearby clusters. Let Y be the $M \times N$ signal matrix. The whitened signal is given by

$$\tilde{Y} = UV^T$$

where

$$Y = USV^T$$

is the singular value decomposition. This is sometimes known as ZCA (zero-phase component analysis) whitening. The new data have an identity covariance matrix and can be calculated by applying the following channel mixing matrix at each time sample:

$$W_{mixing} = US^{-1}U^T$$

This procedure is parallelized by splitting the dataset into time chunks and computing the covariance matrix in the first pass through the data and applying the mixing matrix in a second pass.

Event Detection

As described above, event detection is performed independently on each electrode (as part of its local neighborhood sorting) using the preprocessed (whitened) data. With closely spaced electrodes, it is expected that the same event will be flagged multiple times on different channels, but the subsequent cluster consolidation and fitting stages resolve this redundancy. An event is flagged at time sample t_0 whenever the following two criteria are met:

$$|Y(t_0)| > \mu$$

$$|Y(t_0)| > |Y(t_1)| \text{ for all } |t_0 - t_1| \leq \tau$$

where Y is the preprocessed signal, μ is a detection threshold in units of standard deviations away from the mean, and τ is a detection interval specifying the minimum allowable time difference (in samples) between two events on the same channel. For our datasets we used $\mu = 3$ and $\tau = 10$ which corresponds to *0.33 ms* at our *30 kHz* sampling rate.

While the choice of these parameters is somewhat arbitrary, the detection threshold can be chosen to be quite low (in order to capture low amplitude firing events), with the caveat that the lower the threshold, the greater the computation time. Similarly, with low thresholds, the noise clusters (ultimately discarded) will be larger. Our experience has been that the final sorting results are independent of this choice, provided that it is low enough.

Feature Extraction and the Branch Method

Clustering is performed separately in each electrode neighborhood (typically 5-10 electrodes are used, regardless of total array size). Event clips are extracted, PCA features are computed, and then ISO-SPLIT clustering (described below) is applied in n-dimensional feature space, where n is typically 10. This has the potential to yield in an incorrect cluster merging due to the relatively low dimensionality of the feature space. Therefore, assuming that more than one cluster is found, we recompute the PCA features from the original clips for each initial cluster separately. Clustering is then applied to each of these and the procedure is repeated until no further cluster splitting occurs. In this way, we increase the sensitivity of distinguishing between distinct but nearby clusters. We call this the *branch method*.

At each stage of the branch clustering we use principal component analysis (PCA) features. For each detected time sample t_0, a $M \times T$ clip centered at t_0 is extracted from the preprocessed data. Here M is the number of channels constituting the neighborhood of the electrode of interest, and T is the clip size in samples. We used $T = 50$ throughout. These clips are considered as MT-dimensional vectors and are mapped into the n-dimensional feature space corresponding to the first n principal components. We used $n = 10$ throughout, regardless of the neighborhood size. Again, we note that the effective size of the feature space is larger due to the branch method in which event features are computed recursively.

Clustering via ISO-SPLIT

Clustering takes as input a set of points (n-component vectors) and assigns to each point an integer cluster label. Our efficient, nonparametric clustering method termed ISO-SPLIT is at the heart of the sorting pipeline. It is a density-based method that does not require a tunable scale parameter, nor does it need an a priori estimate for the number of clusters. Instead, a statistical test is applied on one-dimensional projections at each iteration (Magland and Barnett, 2016). This crucial one-dimensional kernel operation (ISO-CUT) is described in a separate section below.

The algorithm is initiated with a fine parcellation (over-clustering) and then the points are redistributed between clusters in successive iterations until convergence (Figure 1B). While in principle the results can depend on the initial parcellation (or clustering), in practice when the parcellation is fine enough, they do not. In fact, a deterministic (albeit more computationally intense) procedure would be obtained by initially assigning each point to its own cluster.

Each iteration then involves pairwise comparisons of nearby clusters. Let A and B be two clusters to be compared. First the points of $A \cup B$ are projected onto a line of optimal discrimination between the two sets. A simple choice, although not always ideal, is to use the line connecting the centroids of A and B. In our implementation, we select an optimal line based on the centroids and the empirical covariance matrices of the sets. Next a statistical test is performed to determine whether this one-dimensional sample is unimodal, or alternatively has two or more modes. This is the ISO-CUT procedure described below. If the unimodality hypothesis is rejected, the data points are redistributed between A and B according to the optimal cut point as determined by ISO-CUT. Otherwise, if unimodality is accepted, then the two clusters are merged.

In order to avoid infinite loops, the algorithm keeps track of which cluster pairs have already been compared. Once all pairs of remaining clusters have been compared, the algorithm is deemed to have converged.

ISO-CUT

The ISO-CUT algorithm (the kernel operation in ISO-SPLIT) is a non-parametric method for testing whether a one-dimensional sample arises from a unimodal distribution and for determining an optimal cut point for clustering. It is similar to the Hartigan dip test for unimodality (Hartigan and Hartigan, 1985) but there are important differences. First, Hartigan's test is only a criterion for accepting/rejecting the unimodality hypthosesis, whereas ISO-CUT also returns an optimal cut point. Second, ISO-CUT uses a maximum-likelihood unimodal approximation to the data, which can be evaluated extremely efficiently using a modified version of isotonic regression. Third, ISO-CUT handles a crucial situation where the Hartigan test fails–that is when a sparse cluster is adjacent to a very dense cluster. This situation arises often in spike sorting as cells can have vastly different firing rates.

Here we present a higher-level description of the algorithm and refer the reader to the Figure S1 and the open source MATLAB and C++ implementations contained in the software itself for the lower-level implementation details. The first step of ISO-CUT is to sort the (assumed distinct) one-dimensional data points so we have $x_1 < x_2 < \ldots < x_n$. Next the maximum-likelihood unimodal fit to the sample is computed. One can show that the density function for the fit is piecewise constant with endpoints at the data points, and that the sequence of values may be obtained using a modified version of isotonic regression, which we call up-down isotonic regression, applied to the reciprocal of the spacings $s_i^{-1} = (x_{i+1} - x_i)^{-1}$. A modified Kolmogorov-Smirnov statistic (Massey, 1951) is then computed to quantify the closeness of the empirical cumulative distribution function to the cumulative distribution function of the unimodal approximation (the modification is needed to handle the important case of sparse clusters on the periphery). If this unitless quantity is above the threshold (we used a value of 1 throughout) then unimodality is rejected.

In the case where the unimodality hypothesis is rejected, ISO-SPLIT returns a cut point, or an optimal cut point between two modes at a point of minimal density (note that the distribution may have more than two modes). Again, we aim to avoid density estimates in selecting such a cut point. Therefore, we employ the non-parametric isotonic regression once again by applying down-up isotonic regressions to the residuals $s_i^{-1} - t_i^{-1}$ where t_i is the estimate of the spacings based on the unimodal approximation. The cut point is taken at the deepest minimum of this sequence within a range of interest. Thus, the optimal cut point is obtained in a non-parametric manner without any density estimates.

Cluster Consolidation across Electrodes

Just as ISO-SPLIT is at the heart of the local clustering, our cluster consolidation strategy (Figure S1B) is the central step for handling the multi-electrode arrays in a nonparametric manner. Since spike sorting is applied separately on each electrode (along with its neighbors), the same neuron is likely to be identified multiple times. In fact, it is expected that the same neural unit will appear on several channels, depending on the density of the electrode array. It is therefore necessary to merge the results across all channels into a single sorting output.

There are several problems with comparing pairs of clusters for potential merging. First, depending on the size and density of the electrode array, and the number of neurons detected on each channel, this could pose a computational challenge. Second, there is a problem with non-transitivity of merge decisions. For example, we could determine that clusters A and B (on different channels) should be merged, and that B and C should be merged, but that A and C should not be merged.

No matter whether merge decisions are based on average waveform shape similarity, coincident firing times, or cluster overlap in feature space, there are other fundamental problems with making such pairwise merge decisions. Consider, for example, the case where clustering on channel 1 is accurate, whereas on channel 2 there is a false merge. Then the corresponding clusters may fail to match up, or the incorrect results of channel 2 may supersede the accuracy on channel 1. This can easily happen when neurons are

closer to the first channel but still give a detectable, but small, signal on the second. A myriad of problematic situations like these can arise.

We therefore propose a different approach – an alternative to merging – which we refer to as *cluster consolidation*. The assumption is that in the majority of cases, a neuron will fire with largest signal on a single primary channel, with the peak signal being lower on neighboring channels. Therefore we retain a cluster $C_{m,i}$ (the i^{th} cluster identified on channel m) if its peak average signal on channel m is sufficiently greater than its peak average signal on every other channel. Otherwise it is considered redundant and is discarded. More precisely, cluster $C_{m,i}$ is retained if for every channel number $m' \neq m$,

$$\max_t \left| W_{m,i}(m,t) \right| > \eta \left| \max_t W_{m,i}(m',t) \right|$$

where $W_{m,i}(m',t)$ is the average spike waveform for cluster $C_{m,i}$ on channel m' and clip sample t, and $\eta < 1$ is a constant. The buffer parameter η (0.9 in this study) is included in order to minimize the chances that the same cluster is eliminated on every channel, and therefore excluded altogether.

Ideally each cluster will be represented exactly once after consolidation. However, sometimes a neuron may yield a very similar peak signal on two adjacent electrodes and may therefore be retained in more than one neighborhood. While this depends on the choice of η and the density of the electrodes, this is a relatively rare occurrence for our datasets.

The goal of the second pass is to remove redundant clusters that survived the first pass of the consolidation (Figure S1). As stated, we need to be careful about non-transitive merge criteria. To be clear, both passes involve only discarding rather than merging redundant clusters. The first step of the second pass is to sort the clusters in order of absolute peak amplitude (of the average spike waveform); if two clusters are determined to be duplicates, then we discard the one with lower absolute peak amplitude. Moving through the sorted list, each cluster is compared with all preceding clusters. Simply, if it is determined that it matches a previous cluster, then it is discarded.

The criteria for two clusters to match are 3-fold: (a) they must have been detected on different channels, otherwise presumably they would not be separated by the clustering; (b) their peak amplitudes must be relatively close (within 30% for this paper), otherwise one would have been discarded in the first pass; (c) they must have a significant number of simultaneous (up to a time deviation threshold) firings (> 50% coincident events for this paper).

ELIMINATING REDUNDANT EVENTS VIA FITTING

While cluster consolidation removes redundant clusters, it can still happen that the same event may be redundantly flagged in more than one neighborhood. For example, if event *a* is correctly included in cluster *A* on channel neighborhood 1, but happens to be incorrectly assigned to cluster *B* on channel neighborhood 2, then, since *A* and *B* are not redundantly associated with the same unit, they will both survive the consolidation stage. However, it is important that each event be included exactly once in the final output. Therefore, the following procedure is used in a final pass to eliminate such redundant events.

In this fitting stage (a multi-pass procedure) we consider each detected event as a candidate. We begin with an empty set of accepted events, and add candidates during multiple sweeps through the data according to whether they reduce the L_2-norm of the residual signal. Let Y be the $M \times N$ signal matrix (recall M is the number of channels and N the number of time samples). On the j^{th} pass, let Y_j be the residual signal (initialized by $Y_1 = Y$). We first compute an L_2-norm reduction score for each candidate event that has not yet been included as follows:

$$S_{j,i} = \sum_{t=1}^{T} \sum_{m=1}^{M} \left(Y_j\left(m, t_0 - \frac{T}{2} + t\right) - W_{k_i}(m,t) \right)^2 - Y_j\left(m, t_0 - \frac{T}{2} + t\right)^2$$

where (t_i, k_i) is the time sample and label for the i^{th} candidate event, $W_k(m,t)$ is the representative waveform for the k^{th} cluster, and T is the clip size (assumed even). The i^{th} event is then included if

$$S_i > 0 \text{ and } S_i > S_j \text{ for all } j \neq i, |i - j| \leq T_0$$

That is, the L_2-norm is reduced by including the event, and the amount by which it is reduced is greater than that of any overlapping candidate event. The waveforms for the newly accepted events are then subtracted from Y_j to obtain a new residual Y_{j+1} and the procedure is repeated until no further changes occur in a pass. To speed things up we keep track of which scores need to be recomputed on subsequent passes.

Partially overlapping events are thus handled properly, assuming that they are at least somewhat separated in either time or space. Note also that the requirement for the score to be positive has the benefit of removing outliers to some extent. Crucially, in contrast to model-based approaches, (Ekanadham et al., 2014; Franke et al., 2015; Pachitariu et al., 2016; Pillow et al., 2013) which use L_2 fitting to update waveform shapes, firing times, and amplitudes, in our scheme L_2 fitting is only used to *eliminate duplicate event*s. In particular, this preserves labels chosen by our non-Gaussian clustering method.

Isolation and Noise Overlap Metrics

Here we describe the post-processing step that classifies "single unit," "noise," and "non-isolated" clusters based on an objective set of criteria, as described above. We have elected *not* to use any firing time information (e.g., dips in cross-correlograms) to make these decisions, so as to leave such information as an independent validation metric. Adhering to our overall approach, we also do not want our metrics to depend on additional assumptions about cluster distributions. Here we define the isolation and noise overlap methods which control automated cluster selection.

First, we describe the isolation metric for assessing how well a cluster

$$A = \{a_1, \ldots, a_n\}$$

is separated from the other clusters. Let A and B be two distinct clusters. For each x in $A \cup B$, let $n_1(x), \ldots, n_k(x)$ be the k nearest neighbors of x in $A \cup B$. Let ρ be the membership function so that $\rho(A) = 1$ and $\rho(B) = 2$. Then we define the k-nearest neighbor overlap between A and B to be

$$m_{overlap}(A,B) = \frac{1}{n}\sum_{j=1}^{n} \frac{\#\{x \in A \cup B : \rho(n_j(x)) = \rho(x)\}}{\#(A \cup B)}$$

which is the fraction of the nearest neighbors that are classified consistently with their parent point. (Often the number of points in one cluster will be much larger than in the other. This can lead to an artificially high overlap metric because the likelihood of misclassification depends not only on the degree of separation but also on the relative sizes of the clusters. Therefore we only sample N random points from each of the two clusters where N is the minimum size of the two clusters. To reduce computation time we also require that N is at most 500.) The isolation metric is then given as

$$m_{isolation}(A) = 1 - \min_{clusters\ B} m_{overlap}(A,B)$$

where the minimum is taken over all other clusters.

We take a somewhat different approach for noise overlap. We define the noise overlap of cluster A to be the overlap metric for A with a "fake" cluster

$$B = \{b_1, \ldots, b_n\}$$

comprised of the same number of random noise events (clips extracted from the original data at purely random times). However, the difficulty in comparing these two clusters is that the event clips of A have a bias in that they were selected for being (perhaps by chance) super-threshold. Therefore, we need to first remove this bias by subtracting out a multiple of the expected noise waveform Z to obtain adjusted clips prior to computing the overlap. We use the following weighted average for the expected noise waveform:

$$Z(m,t) = \frac{\sum_{i=1}^{n} b_i(m_0,t_0) b_i(m,t)}{\sum_{i=1}^{n} b_i(m_0,t_0)}$$

here the weight $b_i(m_0, t_0)$ is the value of the spike at its central channel and central time sample. We then define the noise overlap to be the overlap metric applied to the sets of event clips after projecting out the dimension defined by the expected noise shape:

$$m_{noise}(A) = m_{overlap}\left(\tilde{A}, \tilde{B}\right)$$

Automatic Identification of Bursting Clusters

We use two criteria (waveform similarity and relative timing) to flag a pair of clusters as belonging to the same unit, with one cluster A being labeled as the bursting parent of a second cluster B. First, the average spike waveforms must be similar to one another up to scaling. Here we require that the correlation across time and channels be greater than 0.8 (an adjustable threshold). Second, the cross-correlogram between clusters A and B must have a significant asymmetry within a chosen time window (±15 ms in our analyses) with events in B tending to occur a short time after events in A. This was quantified by comparing n_{after}, the number of B events occurring within 15 ms *after* events in A, to n_{before}, the number of B events occurring within 15 ms before events in A. If n_{after} is significantly greater than $2n_{before}$ ($p < 0.001$, assuming a Poisson distribution), and the correlation criterion is met, then we flag (A,B) as a bursting pair. We note, however, that the output of MountainSort retains the identity of the individual clusters associated with each bursting pair. This maintains data provenance and allows for alternative criteria to be applied at a later date if so desired.

Manual Clustering

Data were bandpass filtered 600-6000 Hz and then thresholded at 60 μv for event detection. Individual units (putative single neurons) were identified by drawing cluster boundaries in two-dimensional projections of peak amplitude, the first two principal components of each channel, peak to trough ratio, or spike width as variables (MatClust, M.P.K.). Only well-isolated neurons with stable spike waveform amplitudes were clustered. Clusters that were cut off at spike threshold were not selected.

Simulations Using Synthetic Data

The datasets used in Figure 6 were generated by superimposing synthetic waveforms on background signal taken from a real dataset. We wanted the background signal to include realistic noise, correlations between channels, and low-amplitude signals from distant neurons. We therefore started with the hippocampal dataset used in this paper, automatically removed time segments that included detectable (relatively high amplitude) spike events and then pieced together the remaining time segments using an overlap region and apodization (a filtering approach to smooth the signal) at the edges of the segments to avoid inflating the noise level on the overlaps.

The shapes of the superimposed spike waveforms were not derived from the sorted dataset because we did not want to bias the results toward whichever sorting algorithm used to obtain those shapes. We also wanted to easily control the number of simulated units and the distribution of peak amplitudes and shapes. Therefore, we created a formula that generated realistic spike shapes dependent on a rise time, peak amplitude, decay time, and recovery time on each of the four channels. We generated units with differing firing rates (randomly selected between 0.5 and 3 spikes per second), different spike waveform shapes, and peak amplitudes ranging from zero to a maximum of 20 standard deviations above the mean, with more units at lower amplitude as reflected in real data.

In the first of the three simulated datasets, 15 units were simulated with around 8 having high enough amplitude to be detected (Figures 6A and 6D). For the second dataset (Figure 6B), 30 units were simulated with around 15 detectable. For the third (Figure 6C), 60 units were simulated with around 30 detectable. The MATLAB scripts for generating these may be found in the source code repository.

Computational Efficiency Measurements

We conducted all processing on a Dell Linux workstation with 192 GB RAM and 40 logical processing cores (Intel Xeon processor 2.8 GHz), although not all cores were used in the experiments, as indicated in the text. All algorithms were implemented as custom C++ programs.

In Vivo Datasets

A total of four 16-channel polymer shanks were targeted to Prelimbic cortex (+ 2.4 to 2.6 AP, ± 1.1 ML, DV −3.4, 7° from sagittal). The tetrode was constructed from four 12.5 μm nichrome wires (California Fine Wire) spun together, with each of the four wires electroplated with gold to an impedance of ∼250 kΩ at 1 kHz. The tetrode was one of sixteen in individual cannulae whose centroid was targeted −3.6 AP, ± 2.4 ML, and then adjusted to CA1 cell layer based on LFP and spiking activity.

For the tetrode dataset, the animal was run for 45 min on the first exposure to the W-track continuous spatial alternation behavior (Frank et al., 2000; Kim and Frank, 2009).

The 16-channel polymer probe dataset was collected during a 7 hr period while the animal was in a 13″ x 13″ walled rest box.

All data were sampled and saved at 30 KHz on a 320-channel modular headstage using Trodes software (SpikeGadgets).

DATA AND SOFTWARE AVAILABILITY

The MountainSort clustering software, as well as the code used to generate the simulated datasets is publically available at: https://github.com/magland/mountainlab. The tetrode dataset is available at: http://dx.doi.org/10.17632/kmmndvycx8.1. The polymer probe dataset is available at: http://dx.doi.org/10.17632/j2mfvnsz2t.1 (part 1/3), http://dx.doi.org/10.17632/ssb8s4766s.1 (part 2/3), and http://dx.doi.org/10.17632/9mgpgn7fsw.1 (part 3 of 3).